Journal of Materials Chemistry C

ROYAL SOCIETY OF CHEMISTRY

PAPER

View Article Online
View Journal | View Issue

Cite this: J. Mater. Chem. C, 2025, 13, 13347

Polymer donors with a new electron-deficient unit for efficient organic solar cells†

Zhe Zhang,‡[a] Tianqi Chen,‡[b] Xuehang Dong,[b] Haoyu Li,[a] Tainan Duan,[c] Ekaterina A. Knyazeva,[d] Alexandra S. Chechulina,[d] Oleg A. Rakitin,[d] Bin Kan,[b] Xiangjian Wan[a] and Yongsheng Chen*[a]

Received 4th April 2025,
Accepted 10th May 2025

DOI: 10.1039/d5tc01406a

rsc.li/materials-c

Polymer donors, as a critical component of the active layer in organic solar cells (OSCs), necessitate the development of high-performance variants to further enhance efficiency. The exploration of novel electron-deficient building blocks plays a pivotal role in driving the sustainable advancement of high-performance polymer donors. In this study, we designed a new electron-deficient unit, dithienobenzobisthiadiazole (DTBBT), and synthesized its corresponding polymer materials (PD-1 and PD-2). Both polymers not only possess wide optical bandgaps exceeding 2.0 eV, but also show deep-lying highest occupied molecular orbital (HOMO) energy levels. When blended with a typical nonfullerene acceptor L8-BO, the PD-2:L8-BO-based binary devices achieved a satisfactory power conversion efficiency (PCE) of 16.34%, which could be attributed to their well-matched energy levels. Remarkably, PD-1-based polymer donors exhibit low non-radiative energy losses of only 0.174 eV in spite of its inferior PCE of 5.52%. Our results highlight DTBBT-based polymer donors as promising candidates for suppressing non-radiative energy losses in OSCs, offering new opportunities for further improving the device performance through molecular engineering.

1. Introduction

Organic solar cells (OSCs), typically composed of a polymer donor and a small molecule acceptor, have emerged as a promising next-generation renewable energy conversion technology due to their advantages of flexibility, light weight and roll-to-roll large-area fabrication.[1–5] Recent advances in nonfullerene acceptors (NFAs) have significantly boosted the performance of OSCs, with power conversion efficiencies (PCEs) now surpassing 20%.[6,7] As a critical component of the active layer in OSCs, polymer donors play a pivotal role in driving progressive improvements in PCE. However, compared with the large number of recently explored NFAs, the development of efficient wide-gap polymer donors is far from sufficient. Generally, an excellent polymer donor tends to meet the following three characteristics:[8–10] (1) a deep highest unoccupied molecular orbital (HOMO) energy level to ensure a high open-circuit voltage (V_{oc}); (2) complementary absorption with NFAs to achieve a high short-circuit current density (J_{sc}); (3) a suitable aggregation behavior to facilitate optimal morphology, thereby improving the fill factor (FF).

To prepare polymer donors with these characteristics, the widely adopted strategy involves copolymerizing the electron-rich donor (D) unit with the electron-deficient acceptor (A) unit, as exemplified by PM6,[11] D18,[12] PBQx-TCl,[13] *etc.* Among the commonly used D units, benzo[1,2-*b*:4,5-*b*′]dithiophene (BDT) with two-dimensional (2D) conjugated side chains stands out due to its rigid skeleton, high hole mobility and structural tunability.[14] However, while halogenated BDT derivatives are prevalent in high-performance polymer donors, the introduction of halogen atoms inevitably complicates synthesis and increases cost, hindering the commercialization of OSCs.[15–17] Typically, the nonhalogenated polymer donors show inferior performance, primarily due to the large voltage loss and weak π–π stacking. Recent studies suggest that copolymerization of nonhalogenated BDT with large conjugations, possessing strong electron-withdrawing A units, can overcome these shortcomings.[18,19] Hence, the development of strong electron-deficient A units to copolymerize with nonhalogenated BDT represents a promising strategy for advancing polymer donor materials.

[a] The Centre of Nanoscale Science and Technology and Key Laboratory of Functional Polymer Materials, Institute of Polymer Chemistry, State Key Laboratory of Elemento-Organic Chemistry, Renewable Energy Conversion and Storage Center (RECAST), Frontiers Science Center for New Organic Matter, College of Chemistry, Nankai University, Tianjin 300071, China. E-mail: yschen99@nankai.edu.cn
[b] School of Materials Science and Engineering, National Institute for Advanced Materials, Nankai University, Tianjin 300350, China
[c] Chongqing Institute of Green and Intelligent Technology, Chongqing School, University of Chinese Academy of Sciences, Chinese Academy of Sciences, China
[d] N. D. Zelinsky Institute of Organic Chemistry, Russian Academy of Sciences, 47 Leninsky Prosp., 119991 Moscow, Russian Federation

† Electronic supplementary information (ESI) available. See DOI: https://doi.org/10.1039/d5tc01406a

‡ These authors contributed equally.

Recently, numerous large fused electron-deficient building blocks, such as dithieno[3′,2′:3,4;2″,3″:5,6]benzo[1,2-*c*][1,2,5]-thiadiazole (DTBT),[12] dithieno[3,2-*f*:2′,3′-*h*]quinoxaline (DTQx),[1,20] dithienoquinoxalineimide (DTQI),[18] and bithiophene imide (BTI),[21] have been successfully employed as A units in high-performance D–A conjugated polymer donors. These conjugation-extended A units have received extensive attention mainly due to their outstanding characteristics:[1,18,20–24] (1) strong electron-withdrawing units (*e.g.*, thiadiazole, quinoxaline, and imide) effectively lower HOMO energy levels to minimize energy losses (E_{loss}); (2) their large coplanar fused aromatics group could enhance π–π stacking and molecular aggregation, promoting efficient intra/intermolecular charge transport. For example, Zhou *et al.*[18] developed a wide band gap polymer donor named QQ1 by copolymerizing the fused electron-deficient DTQI unit with non-halogenated BDT. QQ1 not only possesses a deep HOMO energy level of −5.47 eV, but also shows compact π–π stacking. After blending with polymer acceptor PY-IT and F-BTA3, QQ1-based all-polymer solar cells obtained a record PCE of 19.20%. Meanwhile, Hou *et al.*[13,20,25] explored a series of DTQx-based polymer donors that demonstrated excellent results in polymer and all-polymer solar cells. These advances highlight the great potential of large fused electron-deficient units for developing high-performance polymer donors.

Among numerous electron-deficient units, benzo[1,2-*c*:3,4-*c*′]bis([1,2,5]thiadiazole)[26–29] usually exhibits strong electron-withdrawing capability and compact π–π stacking packing due to its dual thiadiazole configuration and extended coplanar fused structure. Recently, our group successfully incorporated this unit into the conjugated skeleton of NFAs (CH-BBQ and CH-HP),[30,31] which exhibited narrow optical bandgaps, strong crystallinity, and enhanced charge transport properties in blend films, leading to a PCE of over 19%. These promising results inspired us to further explore this unit's potential by designing an extended conjugated derivative dithienobenzobisthiadiazole (DTBBT). Using this novel building block, we developed two wide bandgap polymer donors, namely PD-1 and PD-2, by copolymerizing the DTBBT unit with halogenated BDT or nonhalogenated BDT. Both polymers exhibited wide optical bandgaps, deep-lying HOMO energy levels, and compact molecular packings. However, the PD-1:L8-BO blend-based devices exhibited limited performance with a low PCE of 5.52%, primarily attributed to the suboptimal energy level alignment between PD-1 and L8-BO. In contrast, the PD-2-based device achieved a higher PCE of 16.34%, with a V_{oc} of 0.910 V, a J_{sc} of 25.06 mA cm^{-2}, and an FF of 71.5%, owing to its enhanced efficient exciton dissociation, improved charge transportation, and suppressed charge recombination. Notably, PD-1-based devices demonstrated low non-radiative energy losses (ΔE_3 = 0.174 eV). The results emphasize the great potential of this novel DTBBT block as an effective electron-deficient unit for developing high-performance OSC molecules.

2. Results and discussion

The detailed synthetic route to prepare two polymer donors (PD-1 and PD-2) containing dithienobenzobisthiadiazole is displayed in Scheme S1 (ESI†). The starting compound **1** (4,5-dibromobenzo[1,2-*c*:3,4-*c*′]bis([1,2,5]thiadiazole)) was synthesized based on our previous report.[29] Through Stille coupling between compound **1** and (3,3′-bis(trimethylstannyl)-[2,2′-bithiophene]5,5′-diyl)bis(trimethylsilane), we obtained the key intermediate compound **2**. Subsequent bromination of compound **2** with *N*-bromosuccinimide (NBS) in a mixture of chloroform and trifluoroacetic acid yielded compound **3**. Then, compound **4** was successfully synthesized *via* a palladium-catalyzed Stille coupling reaction, followed by NBS-mediated bromation to produce compound **5**. The structure of all compounds was determined by nuclear magnetic resonance spectroscopy and mass spectrometry. Lastly, two polymer donors PD-1 and PD-2 were prepared by a classic Stille coupling polycondensation reaction between compound **5** with halogenated BDT and compound **5** with nonhalogenated BDT. Structurally, the developed polymer donors PD-1 and PD-2 exhibit strong electron-withdrawing capability, high coplanarity, and robust backbone rigidity compared to existing donor systems, as systematically validated in Fig. S1 (ESI†). The number-average molar masses (M_n) and dispersity ($Đ$) were estimated to be 19.1 kDa/2.77 for PD-1 and 47.7 kDa/2.18 for PD-2 by high-temperature gel permeation chromatography. Both polymer donors dissolved easily in common solvents, such as chloroform (CF), toluene (Tol), chlorobenzene (CB) *etc.*, which could provide a feasible foundation for the fabrication of the devices. Thermal properties of both polymers were investigated by thermogravimetric analysis (TGA) and differential scanning calorimetry (DSC) (Fig. S2, ESI†). The TGA results reveal that PD-2 exhibits superior thermal stability with a higher decomposition temperature than PD-1. Furthermore, DSC measurements show more distinct melting and crystallization peaks for PD-2, indicating stronger intermolecular interactions and more ordered molecular packing compared to PD-1. These observations collectively suggest that PD-2 adopts a more tightly packed aggregation morphology in the solid state.

The UV/vis absorption spectra of PD-1 and PD-2 in diluted solutions and neat films were obtained and are depicted in Fig. S3 (ESI†) and Fig. 1c, with corresponding optical and electrochemical parameters summarized in Table S1 (ESI†). Both polymer donors in solution or film exhibited similar absorption profiles with two obvious absorption regions between 300 and 600 nm. The primary absorption region (450–600 nm) could be attributed to intramolecular charge transfer (ICT) between D and A building blocks, while the short-wavelength features (320–400 nm) could be assigned to localized π–π* transitions. In diluted solutions, PD-1 and PD-2 displayed distinct absorption peaks at 513 nm and 528 nm, respectively, which red-shifted to 522 nm and 565 nm in their thin-film state. As shown in Fig. S4 (ESI†), PD-1 consistently exhibits lower extinction coefficients than PD-2 in both neat and blended films. Compared with PD-2, PD-1 shows a more blue-shifted absorption in solution and film, which indicates that PD-1 possess a weaker ICT effect caused by the introduction of F atoms on the D unit. The absorption edges of PD-1 and PD-2 films located at 609 nm and 613 nm, corresponding to

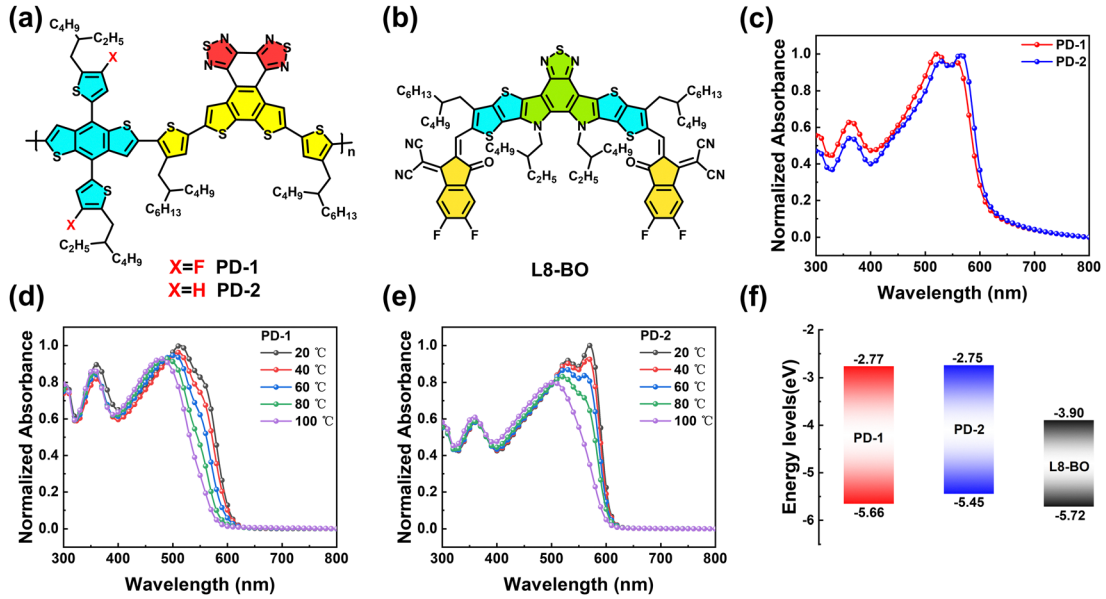

Fig. 1 (a) and (b) The molecular structures of PD-1, PD-2 and L8-BO, respectively; (c) the normalized absorption spectra of PD-1 and PD-2 in the neat film; (d) and (e) the temperature-dependent absorption spectra of PD-1 and PD-2 in chlorobenzene solutions, respectively; (f) the energy level diagrams of PD-1, PD-2 and L8-BO.

their optical bandgaps (E_g^{opt}) of 2.04 and 2.02 eV, respectively. The temperature-dependent UV/vis spectra of both polymer donors in CB solutions were recorded to investigate the molecular aggregation. As shown in Fig. 1d and e, the maximum absorption peaks of both polymers exhibit a large blue-shift when the temperature rises to 100 °C. This phenomenon may imply that the polymer with DTBBT exhibits strong molecular aggregation.[32–34]

Electrochemical cyclic voltammetry (CV) was performed to determine the energy levels of PD-1 and PD-2 (Fig. S4, ESI†), with the resulting energy level diagram presented in Fig. 1f. The lowest unoccupied molecular orbital (LUMO) levels, estimated from the onset of the reduction in their CV curves, are −2.77 eV for PD-1 and −2.75 eV for PD-2, respectively. The HOMO energy levels of PD-1 and PD-2 were determined to be −5.66 eV and −5.45 eV, respectively. These deep-lying HOMO energy levels confirm the strong electron-withdrawing ability of the DTBBT unit. Notably, the F atom on the D unit of PD-1 decreases the LUMO and HOMO energy levels simultaneously. The ΔE_{HOMO} offset between PD-1 and L8-BO is 0.06 eV (<0.1 eV) which may adversely affect the dissociation of excitons, thus leading to low J_{sc} and FF.[3,35,36] In contrast, PD-2 demonstrates optimal compatibility with L8-BO, exhibiting both suitable E_g^{opt} (~2.0 eV) and appropriately positioned HOMO levels (~5.5 eV). Density functional theory (DFT) calculations provided further insight into the molecular orbital distributions (Fig. S5, ESI†). The calculated LUMO and HOMO of PD-1 and PD-2 are −2.58/−4.99 eV, and −2.50/−4.88 eV, which are well consistent with the trend of experimental results. The LUMO of both polymers is primarily localized on the DTBBT unit, while the HOMO exhibits delocalization across the entire polymer backbone.[21] Both polymers exhibit comparably small dihedral angles, indicating enhanced structural planarity in the DTBBT-incorporated polymer backbones.

To evaluate the photovoltaic performance of two polymer donors, the OSCs were fabricated with a conventional device configuration of ITO/PEDOT:PSS/polymer donors:L8-BO/PNDIT-F3N/Ag. The detailed fabrication process and optimization conditions of OSCs are shown in Tables S2–S6 (ESI†). The current density–voltage (J–V) curves of optimal devices are displayed in Fig. 2a, with the corresponding photovoltaic parameters summarized in Table 1. The PD-1:L8-BO based devices exhibited an inferior PCE of 5.52%, characterized by a high V_{oc} of 0.945 V but rather limited J_{sc} (13.43 mA cm^{-2}) and FF (43.6%). In contrast, the PD-2:L8-BO-based devices delivered a high PCE of 16.34%, maintaining a high V_{oc} of 0.910 V while delivering significantly enhanced J_{sc} (25.06 mA cm^{-2}) and FF (71.5%). The enhanced J_{sc} and FF could be ascribed to large driving force and optimal morphology of the PD-2:L8-BO binary blend. Notably, both systems exhibited high V_{oc} values, underscoring DTBBT's exceptional electron-withdrawing capability that deepens HOMO levels, thereby increasing V_{oc} and reducing E_{loss}. To verify the J_{sc} obtained from J–V curves, the external quantum efficiency (EQE) of devices was measured. As can be seen from Fig. 2b, the photo-response range of PD-1-based devices is similar to that of PD-2. However, the PD-2-based devices show significantly stronger photo-response over the entire spectral range, indicative of more efficient exciton dissociation, charge transport, and reduced recombination (discussed below). The calculated J_{sc} values from EQE curves are 12.88 and 24.01 mA cm^{-2} for the PD-1 and PD-2 based devices, respectively, confirming the reliability of the J_{sc} values from J–V curves.

The exciton dissociation and charge recombination behaviors in the two devices were further investigated. First, steady-state photoluminescence (PL) spectroscopy of PD-1 and PD-2 blend films was initially tested. As displayed in Fig. S6 (ESI†),

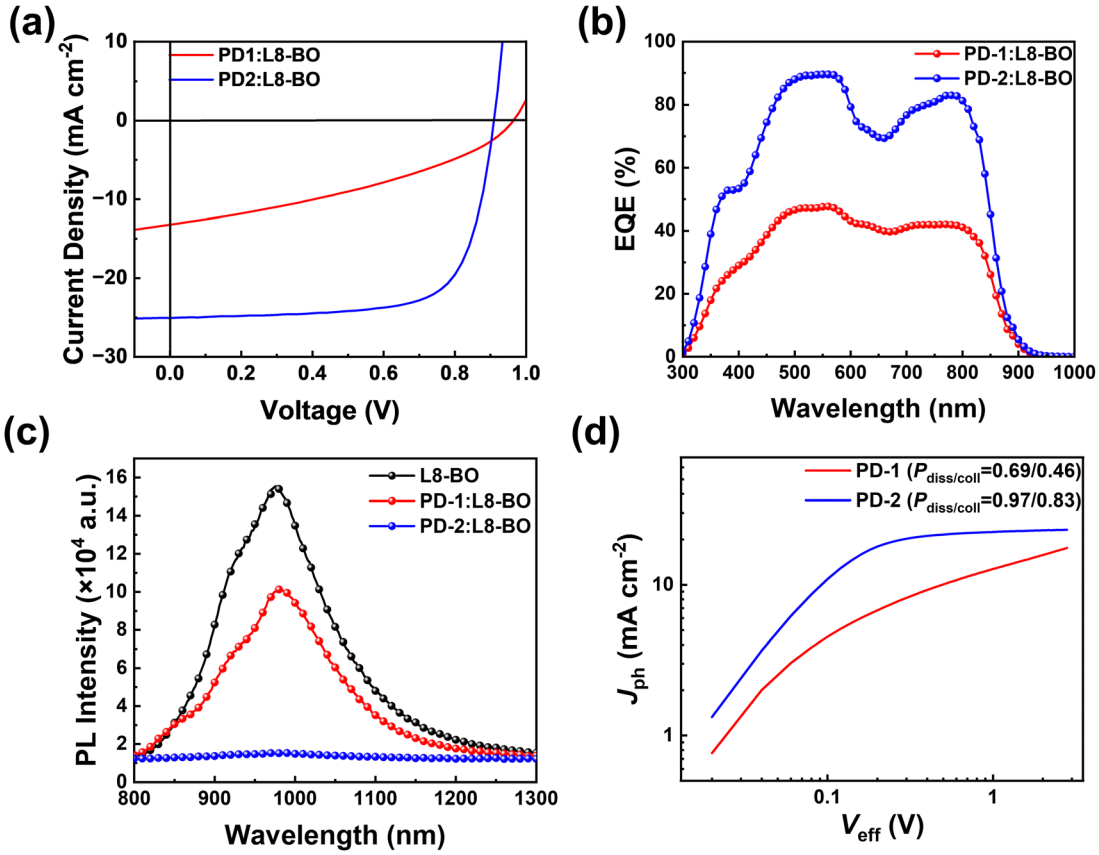

Fig. 2 (a) J–V curves of PD-1- and PD-2-based OSCs; (b) EQE spectra of PD-1- and PD-2-based OSCs; (c) photoluminescence spectra of the L8-BO neat film, PD-1:L8-BO and PD-2:L8-BO blend films; (d) J_{ph}–V_{eff} curves of OSCs.

Table 1 Summary of photovoltaic parameters of OSCs. The average parameters in parentheses were calculated from at least 10 independent devices

Active layer	V_{oc} (V)	J_{sc} (mA cm^{-2})	J_{sc}^{cal} (mA cm^{-2})	FF (%)	PCE (%)
PD-1:L8-BO	0.945 (0.952 ± 0.004)	13.43 (13.55 ± 0.15)	12.88	43.6 (41.7 ± 0.4)	5.52 (5.37 ± 0.07)
PD-2:L8-BO	0.910 (0.907 ± 0.002)	25.06 (25.09 ± 0.12)	24.01	71.5 (70.9 ± 0.6)	16.34 (16.16 ± 0.13)

the PL emission of both polymer donors was quenched by over 90% after blending with L8-BO. The high fluorescence quenching efficiency can be linked to the pronounced charge-separation driving force, originating from a LUMO energy offset exceeding 1 eV. However, upon exciting the L8-BO at 760 nm, the estimated PL quenching efficiency of PD-2:L8-BO is much higher than that of PD-1:L8-BO (90.1% *vs.* 34.5%). The suppressed fluorescence quenching efficiency observed in PD-1:L8-BO blend films may presumably arise from their diminished driving force, as evidenced by a minimal HOMO energy offset ($\Delta E_{HOMO} < 0.1$ eV).[37] Then, the exciton dissociation probability (P_{diss}) and charge collection probability (P_{coll}) were further analyzed by the photocurrent density (J_{ph})–effective voltage (V_{eff}) curves of optimized devices.[38] In Fig. 2d, the J_{ph} of PD-2:L8-BO-based devices is obviously higher than that of PD-1:L8-BO over the total range, indicating that a larger driving force is advantageous for exciton dissociation. P_{diss} and P_{coll} are assessed using the following equations: $P_{diss} = J_{sc}/J_{sat}$ and $P_{coll} = J_{max}/J_{sat.}$, where J_{sat} is the saturated photocurrent density and J_{max} represents the current density at the maximum power output point. Hence, the PD-1:L8-BO-based device afforded P_{diss}/P_{coll} values of 69%/46%. In comparison, the PD-2:L8-BO-based device displayed a P_{diss} of 97% and a P_{coll} of 83%. The higher P_{diss} and P_{coll} of the PD-2:L8-BO system indicate much more exciton dissociation and charge collection of OSCs. The aforementioned results establish that the exciton dissociation of PD-1:L8-BO-based devices is severely constrained, which directly correlates with their inferior photovoltaic performance relative to the PD-2:L8-BO counterpart.

Next, the correlations of J_{sc} and V_{oc} against light intensity (P_{light}) of these devices were further measured to figure out the charge recombination.[39] The bimolecular recombination can be estimated by the relation: $J_{sc} \propto P^{\alpha}$, where the value of α should be 1 if the bimolecular recombination can be completely ignored. The α values for PD-1:L8-BO and PD-2:L8-BO-based devices are 0.98 and 0.99, respectively (Fig. S7, ESI†), indicating

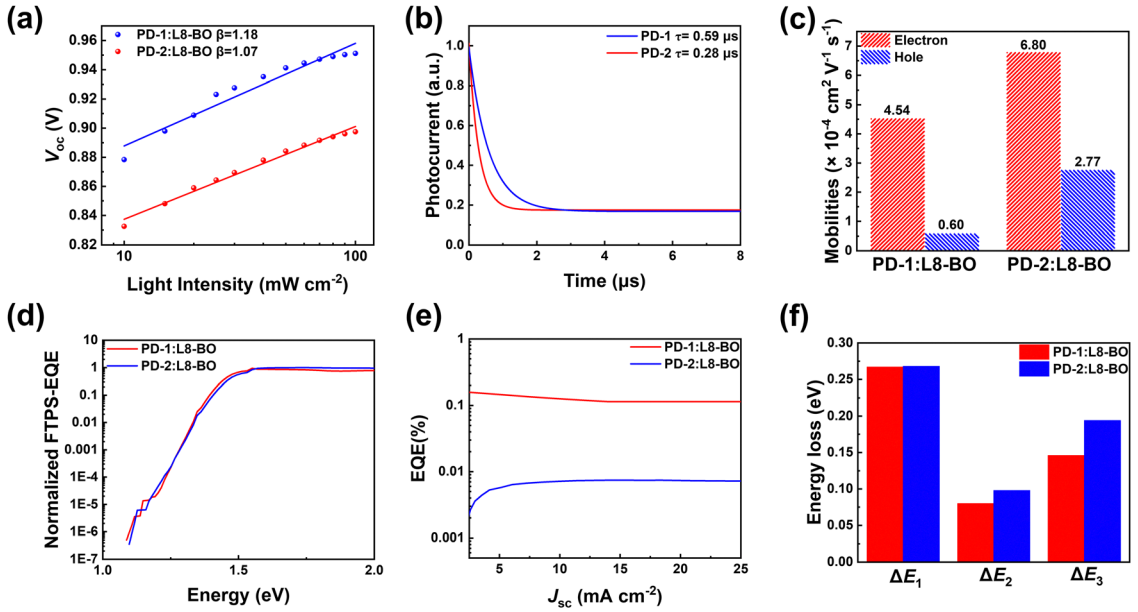

Fig. 3 (a) V_{oc} *vs.* light intensity of the OSCs; (b) transient photocurrent spectra of the OSCs; (c) hole and electron mobilities of the OSCs; (d) Fourier transform photocurrent spectroscopy external quantum efficiency (FTPS-EQE) curves of the OSCs; (e) electro-luminescence external quantum efficiency (EQE_{EL}) curves of the OSCs; (f) energy loss histograms of the OSCs.

that the bimolecular recombination behavior in both devices is greatly suppressed. The dependence of V_{oc} on the P_{light} was tested to provide insight into trap-assisted charge recombination (Fig. 3a). By fitting the V_{oc} and P_{light} data, the slopes (β) of PD-1:L8-BO and PD-2:L8-BO are 1.18 and 1.07, respectively. When the value of β approaches 1, trap-assisted charge recombination can be considered to be completely suppressed. Herein, the PD-2:L8-BO-based devices suffered lower trap-assisted charge recombination than the PD-1:L8-BO-based devices.

The transient photocurrent (TPC) was also performed to evaluate the carrier extraction processes of two devices. As shown in Fig. 3b, the calculated current decay times are 0.59 μs for PD-1:L8-BO-based devices and 0.28 μs for PD-2:L8-BO-based devices. Thus, the charge in PD-2:L8-BO-based devices can be swept out more quickly.[40] Next, the space-charge limited current (SCLC) method was employed to investigate the carrier transport properties of OSCs. As shown in Fig. S8 (ESI†), PD-2 exhibits a higher hole mobility of 3.41×10^{-4} cm^2 V^{-1} s^{-1} compared to PD-1 (1.28×10^{-4} cm^2 V^{-1} s^{-1}). As depicted in Fig. 3c, the electron mobility (μ_e) and hole mobility (μ_h) of PD-1:L8-BO and PD-2:L8-BO blend films are measured to be 4.54×10^{-4}/6.00×10^{-5} cm^2 V^{-1} s^{-1} and 6.80×10^{-4}/2.77×10^{-4} cm^2 V^{-1} s^{-1}, respectively. Moreover, the ratio values of μ_e/μ_h for PD-1:L8-BO and PD-2:L8-BO blend films are 7.57 and 2.45, respectively. The enhanced and balanced carrier mobilities of PD-2:L8-BO blend films facilitate the charge transport and collection, thus leading to their higher J_{sc} and FF.[41]

Finally, to clarify the reasons for the high V_{oc} of the two devices, energy-loss analysis[42] was performed. The Fourier transform photocurrent spectroscopy (FTPS) and EQE_{EL} spectra are displayed in Fig. 3d–f. The corresponding data of energy loss are summarized in Table S7 (ESI†). The total energy loss (E_{loss}) of PD-1:L8-BO and PD-2:L8-BO is estimated to be 0.504 eV and 0.549 eV, respectively. The small E_{loss} of PD-1:L8-BO-based devices may be related to their deeper HOMO energy level. As illustrated in Table S7 (ESI†) and Fig. 3f, the PD-1:L8-BO- and PD-2:L8-BO-based devices show the same ΔE_1 (0.267 eV) due to their similar bandgap. The ΔE_2 values of PD-1:L8-BO and PD-2:L8-BO are 0.080 and 0.098 eV, respectively. Notably, PD-1-based devices have low ΔE_3 values of 0.174 eV. The result means that the newly developed building block (DTBBT) demonstrates considerable potential for minimizing nonradiative recombination energy loss in the OSCs.

Given the significant influence of active layer morphology on photovoltaic performance, atomic force microscopy (AFM) was subsequently employed to investigate the morphological characteristics of blend films.[18,43] The AFM height and phase images are presented in Fig. S9 (ESI†) and Fig. 4. Compared with the PD-1:L8-BO blend film, the PD-2:L8-BO blend film shows a more obvious fibrous network of polymer donors and acceptors (Fig. 4a and b). The root-mean-square (RMS) roughness of PD-1:L8-BO and PD-2:L8-BO blend films was measured to be 1.14 nm and 3.44 nm, respectively. Both blend films exhibit a uniform phase-separated morphology.[44] To study the crystallinity and molecular packing mode in the thin films, grazing incidence wide angle X-ray scattering (GIWAXS) was performed.[45–47] The 2D GIWAXS images and the line-cuts profiles of neat films and blend films are shown in Fig. S10 (ESI†) and Fig. 4c–f, respectively. The corresponding data are comprehensively summarized in Table S8 (ESI†). As shown in Fig. S10 (ESI†), the neat films of PD-1 and PD-2 display a distinct (100) diffraction peak at 0.274 and 0.261 Å^{-1} in the in-plane (IP) direction with *d*-spacings of 22.93 and 24.07 Å, and a clear (010) diffraction peak at 1.72 and 1.65 Å^{-1} in the

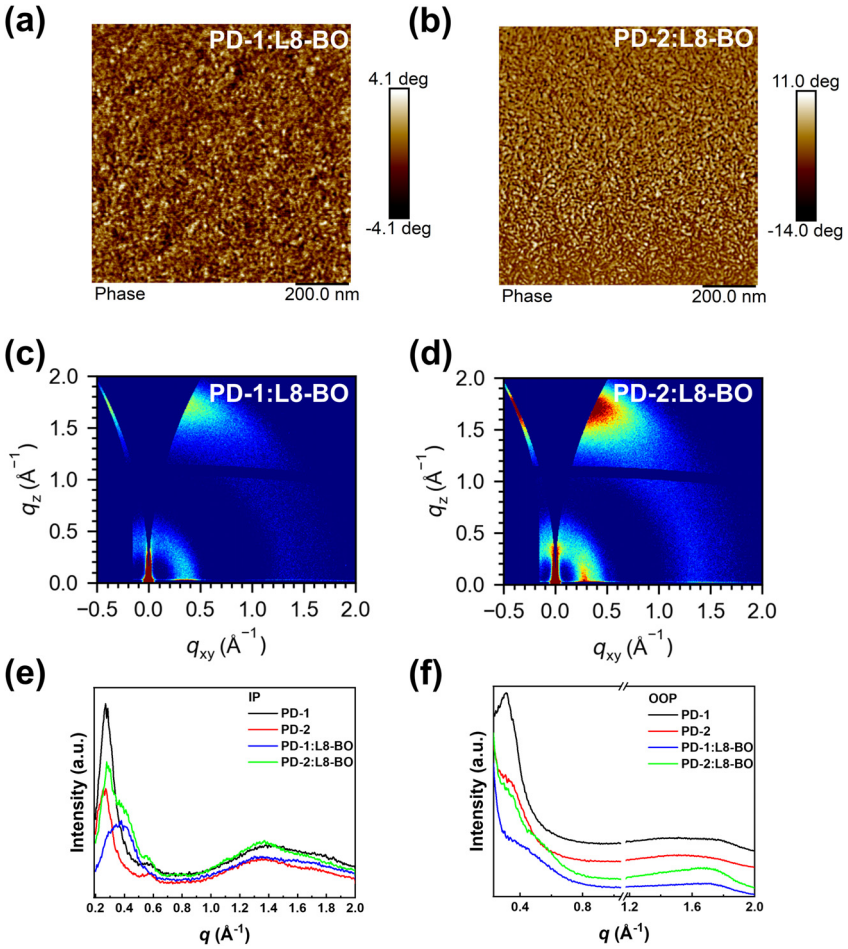

Fig. 4 (a) and (b) AFM phase images of PD-1:L8-BO and PD-2:L8-BO blend films; (c) and (d) 2D GIWAXS patterns of PD1:L8-BO- and PD-2:L8-BO-blend films; (e) line cuts of GIWAXS images of the blend films in the in-plane (IP) direction; (f) line cuts of GIWAXS images of the blend films in the out-of-plane (OOP) direction.

out-of-plane (OOP) direction with *d*-spacings of 3.65 and 3.81 Å, signifying that both polymers exhibit a preferred face-on orientation. The coherence lengths (CLs) of the (010) peaks along the OOP direction are 15.97 Å for PD-1 and 13.03 Å for the PD-2 neat film. Upon blending with L8-BO, both PD-1:L8-BO and PD-2:L8-BO blend films still show a distinctive face-on orientation. As illustrated in Table S8 (ESI†), the *d*-spacings and CLs of the (010) peaks of PD-1:L8-BO and PD-2:L8-BO blend films in the OOP direction are 3.72/15.49 Å and 3.76/8.43 Å, respectively. The small *d*-spacings and large CLs in the PD-1 films could be ascribed to the introduction of the F atom in PD-1, which subsequently reinforced intermolecular interaction.

3. Conclusions

In brief, we have rationally designed and synthesized a novel electron-deficient building block, dithienobenzobisthiadiazole, and subsequently engineered two conjugated polymers (denoted as PD-1 and PD-2) incorporating this strongly electron-withdrawing moiety as the electron acceptor unit. Both PD-1 and PD-2 exhibit notably broad optical bandgaps (>2.0 eV) coupled with deep-lying HOMO energy levels, which are particularly advantageous for achieving enhanced V_{oc} in photovoltaic devices. However, the fluorinated derivative PD-1 exhibits an excessively deep HOMO level (−5.66 eV), which detrimentally compromises the exciton dissociation driving force (ΔHOMO < 0.1 eV). This fundamental mismatch results in significantly diminished device performance (PCE = 5.52%, J_{sc} = 12.88 mA cm^{-2}). Instead, PD-2 synthesized *via* copolymerization with the non-halogenated BDT unit, demonstrates optimal energetic alignment with L8-BO, which facilitates efficient exciton dissociation. Consequently, the PD-2-based binary device achieved a champion PCE of 16.34%, with a V_{oc} of 0.910 V, a J_{sc} of 25.06 mA cm^{-2}, and an FF of 71.5%. Notably, polymer donor PD-1 demonstrates low non-radiative energy losses (ΔE_3 = 0.174 eV). Hence, our work demonstrates that the DTBBT unit could serve as a promising electron-deficient building block for donor materials in high open-circuit voltage devices, and further molecular innovation based on this novel DTBBT unit is undergoing.

Author contributions

Zhe Zhang: conceptualization, investigation, visualization, methodology, formal analysis and writing – original draft;

Tianqi Chen: investigation, visualization, methodology; Xuehang Dong: investigation and formal analysis; Haoyu Li: formal analysis and data curation; Tainan duan: conceptualization, methodology, and formal analysis; E. A. Knyazeva: investigation and methodology; A. S. Chechulina: investigation and validation; O. A. Rakitin: supervision and resources; Bin Kan: review & editing, validation, supervision; Xiangjian Wan: resources, project administration, formal analysis, conceptualization; Yongsheng Chen: writing – review & editing, visualization, validation, project administration, methodology, formal analysis, conceptualization. The manuscript was written through contributions from all authors. All authors have given approval to the final version of the manuscript.

Data availability

The data supporting this article have been included as part of the ESI.†

Conflicts of interest

The authors declare no conflict of interest.

Acknowledgements

The authors gratefully acknowledge the financial support from the Ministry of Science and Technology of the People's Republic of China (2023YFE0210400), the National Natural Science Foundation of China (22361132530, 52025033, and 52303237), the Natural Science Foundation of Tianjin (24JCYBJC01540), and the Russian Science Foundation (grant no. 24-43-00022).

References

1 H. Liu, Y. Geng, Z. Xiao, L. Ding, J. Du, A. Tang and E. Zhou, *Adv. Mater.*, 2024, **36**, 2404660.
2 P. Ding, D. Yang, S. Yang and Z. Ge, *Chem. Soc. Rev.*, 2024, **53**, 2350–2387.
3 J. Wang, Y. Xie, K. Chen, H. Wu, J. M. Hodgkiss and X. Zhan, *Nat. Rev. Phys.*, 2024, **6**, 365–381.
4 S. Li, Z. Li, X. Wan and Y. Chen, *eScience*, 2023, **3**, 100085.
5 G. Wang, M. A. Adil, J. Zhang and Z. Wei, *Adv. Mater.*, 2018, **31**, 1805089.
6 C. Li, J. Song, H. Lai, H. Zhang, R. Zhou, J. Xu, H. Huang, L. Liu, J. Gao, Y. Li, M. H. Jee, Z. Zheng, S. Liu, J. Yan, X.-K. Chen, Z. Tang, C. Zhang, H. Y. Woo, F. He, F. Gao, H. Yan and Y. Sun, *Nat. Mater.*, 2025, **24**, 433–443.
7 H. Chen, Y. Huang, R. Zhang, H. Mou, J. Ding, J. Zhou, Z. Wang, H. Li, W. Chen, J. Zhu, Q. Cheng, H. Gu, X. Wu, T. Zhang, Y. Wang, H. Zhu, Z. Xie, F. Gao, Y. Li and Y. Li, *Nat. Mater.*, 2025, **24**, 444–453.
8 Y. Liu, B. Liu, C.-Q. Ma, F. Huang, G. Feng, H. Chen, J. Hou, L. Yan, Q. Wei, Q. Luo, Q. Bao, W. Ma, W. Liu, W. Li, X. Wan, X. Hu, Y. Han, Y. Li, Y. Zhou, Y. Zou, Y. Chen, Y. Li, Y. Chen, Z. Tang, Z. Hu, Z.-G. Zhang and Z. Bo, *Sci. China: Chem.*, 2021, **65**, 224–268.
9 J.-S. Wu, S.-W. Cheng, Y.-J. Cheng and C.-S. Hsu, *Chem. Soc. Rev.*, 2015, **44**, 1113–1154.
10 J. Yi, G. Zhang, H. Yu and H. Yan, *Nat. Rev. Mater.*, 2023, **9**, 46–62.
11 M. Zhang, X. Guo, W. Ma, H. Ade and J. Hou, *Adv. Mater.*, 2015, **27**, 4655–4660.
12 Q. Liu, Y. Jiang, K. Jin, J. Qin, J. Xu, W. Li, J. Xiong, J. Liu, Z. Xiao, K. Sun, S. Yang, X. Zhang and L. Ding, *Sci. Bull.*, 2020, **65**, 272–275.
13 Y. Xu, Y. Cui, H. Yao, T. Zhang, J. Zhang, L. Ma, J. Wang, Z. Wei and J. Hou, *Adv. Mater.*, 2021, **33**, 2101090.
14 H. Yao, L. Ye, H. Zhang, S. Li, S. Zhang and J. Hou, *Chem. Rev.*, 2016, **116**, 7397–7457.
15 T. Zhang, C. An, Y. Cui, J. Zhang, P. Bi, C. Yang, S. Zhang and J. Hou, *Adv. Mater.*, 2022, **34**, 2105803.
16 T. Jia, J. Zhang, H. Tang, J. Jia, K. Zhang, W. Deng, S. Dong and F. Huang, *Chem. Eng. J.*, 2022, **433**, 133575.
17 L. Wang, T. Wang, J. Oh, Z. Yuan, C. Yang, Y. Hu, X. Zhao and Y. Chen, *Chem. Eng. J.*, 2022, **442**, 136068.
18 Z. Wang, X. Wang, L. Tu, H. Wang, M. Du, T. Dai, Q. Guo, Y. Shi and E. Zhou, *Angew. Chem., Int. Ed.*, 2024, **63**, e202319755.
19 X. Yuan, B. Zhang, Y. Li, F. Zhao, W. Wei, Y. Zhang, J. Li, Y. Tian, Z. Ma, Z. Tang, Z. Liu, F. Huang, Y. Cao and C. Duan, *ACS Appl. Mater. Interfaces*, 2025, **17**, 6659–6667.
20 J. Wang, Y. Cui, Y. Xu, K. Xian, P. Bi, Z. Chen, K. Zhou, L. Ma, T. Zhang, Y. Yang, Y. Zu, H. Yao, X. Hao, L. Ye and J. Hou, *Adv. Mater.*, 2022, **34**, 2205009.
21 M. An, Q. Liu, S. Y. Jeong, B. Liu, E. Huang, Q. Liang, H. Li, G. Zhang, H. Y. Woo, L. Niu, X. Guo and H. Sun, *Angew. Chem., Int. Ed.*, 2024, **63**, e202410498.
22 M. Pu, X. Lai, H. Chen, C. Cao, Z. Wei, Y. Zhu, L. Tian and F. He, *J. Energy Chem.*, 2023, **77**, 19–26.
23 J. Chen, D. Li, M. Su, Y. Xiao, H. Chen, M. Lin, X. Qiao, L. Dang, X. C. Huang, F. He and Q. Wu, *Angew. Chem., Int. Ed.*, 2023, **62**, e202215930.
24 M. Su, M. Lin, S. Mo, J. Chen, X. Shen, Y. Xiao, M. Wang, J. Gao, L. Dang, X.-C. Huang, F. He and Q. Wu, *ACS Appl. Mater. Interfaces*, 2023, **15**, 37371–37380.
25 Y. Xiao, H. Yao, J. Wang, T. Zhang, Z. Chen, J. Qiao, N. Yang, Y. Yu, J. Ren, Z. Li, X. Hao and J. Hou, *Adv. Energy Mater.*, 2024, **14**, 2400928.
26 C. M. Cillo and T. D. Lash, *J. Heterocycl. Chem.*, 2009, **41**, 955–962.
27 M. Müller, S. Koser, O. Tverskoy, F. Rominger, J. Freudenberg and U. H. F. Bunz, *Chem. – Eur. J.*, 2019, **25**, 6082–6086.
28 S. Mataka, Y. Ikezaki, Y. Shimojo, M. Tashiro and A. Tori, *Chem. Ber.*, 2006, **126**, 2767–2769.
29 A. S. Chechulina, L. S. Konstantinova, N. V. Obruchnikova, E. A. Knyazeva, B. Kan, T. Duan, Y. Chen, R. A. Aysin and O. A. Rakitin, *Chem. Heterocycl. Compd.*, 2024, **60**, 403–408.
30 T. Duan, W. Feng, Y. Li, Z. Li, Z. Zhang, H. Liang, H. Chen, C. Zhong, S. Jeong, C. Yang, S. Chen, S. Lu, O. A. Rakitin,

C. Li, X. Wan, B. Kan and Y. Chen, *Angew. Chem., Int. Ed.*, 2023, **62**, e202308832.
31 T. Duan, J. Wang, X. Zuo, X. Bi, C. Zhong, Y. Li, Y. Long, K. Tu, W. Zhang, K. Yang, H. Zhou, X. Wan, Y. Zhao, B. Kan and Y. Chen, *Mater. Horiz.*, 2024, **11**, 4413–4423.
32 J. Du, K. Hu, J. Zhang, L. Meng, J. Yue, I. Angunawela, H. Yan, S. Qin, X. Kong, Z. Zhang, B. Guan, H. Ade and Y. Li, *Nat. Commun.*, 2021, **12**, 5264.
33 R. Steyrleuthner, M. Schubert, I. Howard, B. Klaumunzer, K. Schilling, Z. Chen, P. Saalfrank, F. Laquai, A. Facchetti and D. Neher, *J. Am. Chem. Soc.*, 2012, **134**, 18303–18317.
34 J. Clark, J.-F. Chang, F. C. Spano, R. H. Friend and C. Silva, *Appl. Phys. Lett.*, 2009, **94**, 163306.
35 Y. Liu, B. Liu, C.-Q. Ma, F. Huang, G. Feng, H. Chen, J. Hou, L. Yan, Q. Wei, Q. Luo, Q. Bao, W. Ma, W. Liu, W. Li, X. Wan, X. Hu, Y. Han, Y. Li, Y. Zhou, Y. Zou, Y. Chen, Y. Liu, L. Meng, Y. Li, Y. Chen, Z. Tang, Z. Hu, Z.-G. Zhang and Z. Bo, *Sci. China: Chem.*, 2022, **65**, 1457–1497.
36 R. S. Gurney, D. G. Lidzey and T. Wang, *Rep. Prog. Phys.*, 2019, **82**, 036601.
37 J. Zhang, C. H. Tan, K. Zhang, T. Jia, Y. Cui, W. Deng, X. Liao, H. Wu, Q. Xu, F. Huang and Y. Cao, *Adv. Energy Mater.*, 2021, **11**, 2102559.
38 K. Zhang, Z. Liu and N. Wang, *J. Power Sources*, 2019, **413**, 391–398.
39 S. R. Cowan, A. Roy and A. J. Heeger, *Phys. Rev. B: Condens. Matter Mater. Phys.*, 2010, **82**, 245207.
40 M. Babics, R.-Z. Liang, K. Wang, F. Cruciani, Z. Kan, M. Wohlfahrt, M.-C. Tang, F. Laquai and P. M. Beaujuge, *Chem. Mater.*, 2018, **30**, 789–798.
41 C. M. Proctor, J. A. Love and T. Q. Nguyen, *Adv. Mater.*, 2014, **26**, 5957–5961.
42 S. Liu, J. Yuan, W. Deng, M. Luo, Y. Xie, Q. Liang, Y. Zou, Z. He, H. Wu and Y. Cao, *Nat. Photonics*, 2020, **14**, 300–305.
43 Q. Yang, W. Yu, J. Lv, P. Huang, G. He, Z. Xiao, Z. Kan and S. Lu, *Dyes Pigm.*, 2022, **200**, 110180.
44 F. Zhao, C. Wang and X. Zhan, *Adv. Energy Mater.*, 2018, **8**, 1703147.
45 J. L. Baker, L. H. Jimison, S. Mannsfeld, S. Volkman, S. Yin, V. Subramanian, A. Salleo, A. P. Alivisatos and M. F. Toney, *Langmuir*, 2010, **26**, 9146–9151.
46 A. Hexemer, W. Bras, J. Glossinger, E. Schaible, E. Gann, R. Kirian, A. MacDowell, M. Church, B. Rude and H. Padmore, *J. Phys.: Conf. Ser.*, 2010, **247**, 012007.
47 J. Rivnay, S. C. Mannsfeld, C. E. Miller, A. Salleo and M. F. Toney, *Chem. Rev.*, 2012, **112**, 5488–5519.

